Progress In Electromagnetics Research M, Vol. 95, 35–44, 2020

Analysis of Radiation Field Excited by a Vertical Electric Dipole in a Four-Layered Region

Zhuhong Lin[1], Zhiyi Gao[2], Qihang Wang[1], and Yan Li[3, 4, *]

Abstract—Electric dipoles are the fundamental components of a planar multi-layered circuit. Present work focuses on the theoretical investigations of radiation field due to a vertical electric dipole in a four-layered region composed of a perfect conductor covered with two dielectrics and the air above. Locating a vertical electric dipole (VED) on or near the air-dielectric boundary, approximate formulas are obtained. The resultant analytical formulas have the merit of offering unique insights about the characteristics of the radiation field including direct waves, reflect waves, lateral waves, and trapped surface waves. The amplitude of the field along the boundary exhibits the dependence of $\rho^{-1/2}$, which is an intrinsic characteristic of trapped surface waves, where ρ is the propagation distance. In addition, the radiation field is further examined for propagation distance and propagation characteristics of the interference phenomenon. Furthermore, when the observation angle $\Theta \geq 88^{\circ}$, the lateral wave still exists; however, the trapped surface wave is a major component of the total field. The proposed formulas have potential to develop planar four-layered circuit structures.

1. INTRODUCTION

Electromagnetic (EM) field excited by an electric dipole in layered media has been studied over a century due to its applications in through-the-Earth communication, underwater communication, ground penetrating radar technology, and antenna. The problem dates back to the classic paper in which Sommerfeld started to investigate the EM field of a vertical electric dipole (VED) on the boundary between a two-layered region [1]. Subsequently, significant developments have been worked out in a three-layered region based on the results of two-layered media. The findings were well summarized in two famous monographs by Wait [2] and King et al. [3]. In the 1990s, comments by Wait [4] and Mahmoud et al. [5] claimed that King and Sandler's work [6–8] overlooked the trapped surface wave, which varies as $\rho^{-1/2}$ in far-field and should be considered.

Debates have received substantial interest, and much research has been explored. When the source and observation point are both on the surface, the method proposed by [9–11] is more accurate. This method incorporates the fact that trapped surface wave, determined by the residue sums of the poles, can be excited efficiently by VED/HED in a three-layered regions and should not be neglected. To extend the study, analytical expressions of the EM field generated by VED were obtained in a four-layered medium using a similar method [12, 13]; correspondingly, details were summarized in the book of Li [14]. Meanwhile, with further research, a four-layered model was used in many situations, and

Received 19 May 2020, Accepted 21 July 2020, Scheduled 4 August 2020
* Corresponding author: Yan Li (liyan@cjlu.edu.cn).
Note: Zhuhong Lin and Zhiyi Gao contributed to the work equally and should be regarded as co-first authors.
[1] College of Information Science and Electronic Engineering, Zhejiang University, Yuquan Campus, Hangzhou, Zhejiang Province 310027, China. [2] State Key Laboratory of Reliability and Intelligence of Electrical Equipment and Key Laboratory of Electromagnetic Field and Electrical Apparatus Reliability, Hebei University of Technology, Tianjing, Hebei Province 300130, China. [3] Key Laboratory of Electromagnetic Wave Information Technology and Metrology of Zhejiang Province, College of Information Engineering, China Jiliang University, Hangzhou, Zhejiang Province 310027, China. [4] Zhejiang Provincial Key Laboratory of Advanced Microelectronic Intelligent Systems and Applications, Hangzhou, Zhejiang Province 310027, China.

many viable solutions have found. The dyadic Green function was applied to examine the EM field in a four-layered forest environment [15, 16]. Approximate formulas were generated by HED buried in a four-layered media using generalized reflection coefficients [17] presented by Lu et al., which indicated that the trapped surface wave and the lateral wave propagate along the air-dielectric boundary and between two dielectric layers. Recently, Zou used lateral wave in a four-layered model for interlayer debonding detection in asphalt airport pavement [18]. The problem addressed in this paper parallels the analysis carried out in published work on the EM field of the horizontal electric dipole (HED) [19]. The actual formulas are, of course, quite different. The VED located in the dielectric substrate is the element for all connections to the metal ground plane from circuit elements and transmission lines on the substrate. However, most existing research has focused on design and numerical methods, while the theoretical treatment for the VED applicable to microstrip antenna is still lacking, thus the motivation to study the present problem.

The aims of this paper are twofold: 1) Since the far-field behavior is most conveniently expressed in spherical coordinates, the corresponding analytical expressions are derived and analyzed. 2) Computation and analysis are carried out for propagation mechanism of radiation filed, propagation distance, angular degrees, and the thickness of the dielectric layer. In Section 2, the radiation field is derived with the asymptotic method and relations between cylindrical and spherical coordinates. In Section 3, numerical results are developed. Two different cases are considered to demonstrate the properties of the trapped surface wave contributions. In addition, the propagation distance, thickness of the dielectric layer, relative permittivities, and observation angle (Θ) are taken into consideration. In Section 4, conclusions are drawn.

2. METHODOLOGY

2.1. Far-Field Solutions in a Four-Layered Region

The 3D geometry in spherical coordinates is illustrated in Fig. 1. The vertical electric dipole in the $\hat{z}$ direction is located at $(0, 0, d)$. Region j $(j = 0, 1, 2, 3)$ is the air layer, dielectric layer, dielectric layer, and a perfect conductor, respectively. Region j $(j = 0, 1, 2)$ is characterized by the permeability μ_0,

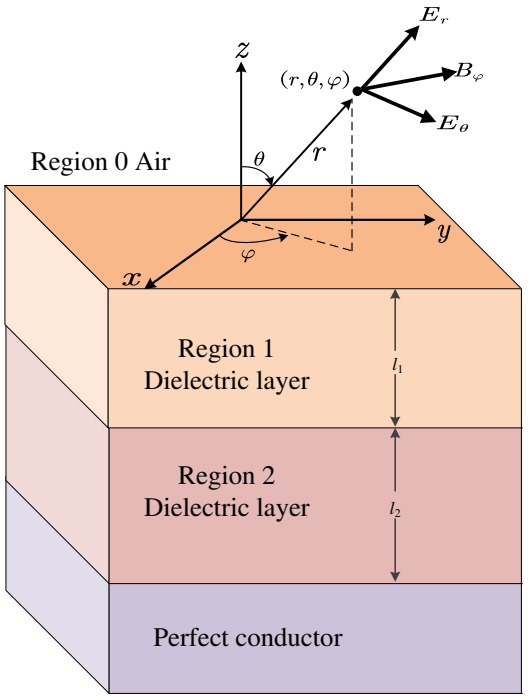

Figure 1. Geometry of VED in a four-layered region.

permittivity ϵ_j, and conductivity σ_j, respectively. The thicknesses of the dielectric layers are l_1 and l_2. Therefore, the wave numbers of the four-layered region can be expressed as:

$$\begin{aligned} k_0 &= \omega\sqrt{\mu_0\epsilon_0} \\ k_j &= \omega\sqrt{\mu_0(\epsilon_0\epsilon_{jr} + i\sigma_j/\omega)}, \quad j = 1, 2 \\ k_3 &\to \infty \end{aligned} \tag{1}$$

In this paper, the time harmonic factor is $e^{-i\omega t}$. The EM field in a four-layered region containing Sommerfeld integral form can be expressed as follows:

$$E_{0\rho}(\rho,\varphi) = \frac{i\omega\mu_0}{4\pi k_0^2}\int_0^\infty \left[\pm e^{i\gamma_0|z-d|} + e^{i\gamma_0(z+d)} - (Q+1)e^{i\gamma_0(z+d)}\right] J_1(\lambda\rho)\lambda^2 d\lambda \tag{2}$$

$$E_{0z}(\rho,\varphi) = -\frac{\omega\mu_0}{4\pi k_0^2}\int_0^\infty \gamma_0^{-1}\left[e^{i\gamma_0|z-d|} + e^{i\gamma_0(z+d)} - (Q+1)e^{i\gamma_0(z+d)}\right] J_0(\lambda\rho)\lambda^3 d\lambda \tag{3}$$

$-Q$ is defined as:

$$-Q = \frac{\gamma_0 - \dfrac{k_0^2}{\omega\mu_0}Z_{s0}(0)}{\gamma_0 + \dfrac{k_0^2}{\omega\mu_0}Z_{s0}(0)} \tag{4}$$

Here, Z_{s0} is the surface impedance.

$$Z_{s0} = \frac{\omega\mu_0\gamma_1}{k_1^2}\tanh\left[-i\gamma_1 l_1 + \tanh^{-1}\left[\left(\frac{\gamma_2 k_1^2}{\gamma_1 k_2^2}\right)\tanh\left[-i\gamma_2 l_2 + \tanh^{-1}\left(\frac{\gamma_3 k_2^2}{\gamma_2 k_3^2}\right)\right]\right]\right] \tag{5}$$

When $k_3 \to \infty$, Q is simplified to:

$$Q = -\frac{\gamma_0 + \dfrac{k_0^2}{\omega\mu}\dfrac{i\omega\mu_0\gamma_1}{k_1^2}\dfrac{\gamma_1 k_2^2\tan\gamma_1 l_1 + \gamma_2 k_1^2\tan\gamma_2 l_2}{\gamma_1 k_2^2 - \gamma_2 k_1^2\tan\gamma_1 l\tan\gamma_2 l_2}}{\gamma_0 - \dfrac{k_0^2}{\omega\mu}\dfrac{i\omega\mu_0\gamma_1}{k_1^2}\dfrac{\gamma_1 k_2^2\tan\gamma_1 l_1 + \gamma_2 k_1^2\tan\gamma_2 l_2}{\gamma_1 k_2^2 - \gamma_2 k_1^2\tan\gamma_1 l\tan\gamma_2 l_2}} \tag{6}$$

The formulas for EM field in a four-layered region were obtained by Xu [13].

$$\begin{aligned} E_{0\rho}(\rho,z) &= -\frac{\omega\mu_0}{4\pi k_0}\left[e^{ik_0 r_1}\left(\frac{ik_0\rho}{r_1^2}\right)\left(\frac{z-d}{r_1}\right) + e^{ik_0 r_2}\left[\left(\frac{ik_0\rho}{r_2^2}\right)\left(\frac{z+d}{r_2} + 2\epsilon^*\frac{r_2^2}{\rho^2}\right) + 2\epsilon^* T^*\right]\right] \\ &\quad -\omega\mu_0\sqrt{\frac{1}{2\pi\rho}}e^{-i\frac{\pi}{4}}\sum_j \frac{A(\lambda_j)(\lambda_j^*)^{3/2}}{q'(\lambda_j^*)}e^{i\gamma_0(\lambda_j^*)(z+d)+i\lambda_j^*\rho} \end{aligned} \tag{7}$$

$$\begin{aligned} E_{0z}(\rho,z) &= \frac{\omega\mu_0}{4\pi k_0}\left[e^{ik_0 r_1}\left(\frac{ik_0}{r_1}\right)\left(\frac{\rho}{r_1}\right)^2 + e^{ik_0 r_2}\left[\frac{ik_0}{r_2}\left(\frac{\rho}{r_2}\right) + 2T^*\right]\right] \\ &\quad +\omega\mu_0\sqrt{\frac{1}{2\pi\rho}}e^{-i\frac{\pi}{4}}\sum_j \frac{A(\lambda_j)(\lambda_j^*)^{5/2}}{q'(\lambda_j^*)\gamma_0(\lambda_j^*)}e^{i\gamma_0(\lambda_j^*)(z+d)+i\lambda_j^*\rho} \end{aligned} \tag{8}$$

In Equations (7) and (8), $q'(\lambda)$ represents the derivations of the pole equations, where λ refers to the roots. The solutions to λ rely on piece-wise root-finding algorithms combined with the Newton-Raphson method, which is more accurate than the graphical approach used in [13].

$$\begin{aligned} q'(\lambda) = &-k_1^2\frac{\lambda}{\gamma_0}(\gamma_1 k_2^2 - \gamma_2 k_1^2\tan\gamma_1 l_1\tan\gamma_2 l_2) + ik_0^2\frac{\lambda}{\gamma_1}(\gamma_1 k_2^2\tan\gamma_1 l_1 + \gamma_2 k_1^2\tan\gamma_2 l_2) \\ &+ k_1^2\gamma_0\left[-\frac{\lambda}{\gamma_1}k_2^2 + \frac{\lambda}{\gamma_2}k_1^2\tan\gamma_1 l_1\tan\gamma_2 l_2 + k_1^2\gamma_2\lambda\left(\frac{l_1}{\gamma_1}\sec^2\gamma_1 l_1\tan\gamma_2 l_2 + \frac{l_2}{\gamma_2}\sec^2\gamma_2 l_2\tan\gamma_1 l_1\right)\right] \\ &+ ik_0^2\gamma_1\lambda\left(\frac{k_2^2\tan\gamma_1 l_1}{\gamma_1} + \frac{k_1^2\tan\gamma_2 l_2}{\gamma_2} + k_2^2 l_1\sec^2\gamma_1 l_1 + k_1^2 l_1\sec^2\gamma_2 l_2\right) \end{aligned} \tag{9}$$

$$\gamma_n = \sqrt{k_n^2 - \lambda_j}, \quad n = 0, 1, 2$$

Following the above formulas, other parameters are defined as:

$$\epsilon^* = i\frac{k_0}{k_1^2}\gamma_{10}\frac{\gamma_{10}k_2^2\tan(\gamma_{10}l_1)+\gamma_{20}k_1^2\tan(\gamma_{20}l_2)}{\gamma_{10}k_2^2-\gamma_{20}k_1^2\tan(\gamma_{10}l_1)\tan(\gamma_{20}l_2)} \tag{10}$$

$$A(\lambda_j) = k_2^2\gamma_1^2(\lambda_j^*)\tan\gamma_1(\lambda_j^*)l_1 + k_1^2\gamma_1(\lambda_j^*)\gamma_2(\lambda_j^*)\tan\gamma_2(\lambda_j^*)l_2 \tag{11}$$

$$r_1 = \sqrt{\rho^2+(z-d)^2}, \quad r_2 = \sqrt{\rho^2+(z+d)^2} \tag{12}$$

In formula (12), r_1 and r_2 represent the distance between source point and observation point. Upper sign + and lower sign − correspond to the source point and mirror source point, respectively.

2.2. Asymptotic Method

When the far region condition $k_0\rho \geq 1$ is satisfied, the condition $|P^*| \geq 4$ is established. The Fresnel-integral term is approximated as the form with:

$$P^* = \frac{k_0\rho}{2}\left(\frac{z+d}{\rho}+\epsilon^*\right)^2 \tag{13}$$

$$T^* = k_0^2\sqrt{\frac{\pi}{k_0\rho}}\,\epsilon^* e^{-iP^*}F(P^*) \to \frac{ik_0\rho}{\rho^2}\frac{\epsilon^*}{\epsilon^*+(z+d)/\rho}+\frac{\epsilon^*}{\rho^2}\left[\frac{1}{\epsilon^*+(z+d)/\rho}\right]^3 \tag{14}$$

where the Fresnel integral $F(P^*)$ is defined by:

$$F(P^*) = \frac{1}{2}(1+i) - \int_0^{P^*}\frac{e^{it}}{(2\pi t)^{1/2}}dt \tag{15}$$

It is possible to express the electromagnetic field in spherical coordinates (r_0, Θ, Φ) with substitutions.

$$r_0 = \sqrt{\rho^2+z^2}, \quad \sin\Theta = \frac{\rho}{r_0}, \quad \cos\Theta = \frac{z}{r_0} \tag{16}$$

Taking into account $d^2 \ll r_0^2$, therefore, r_1 and r_2 must be approximated, $r_1 \sim r_0 - d\cos\Theta$, $r_2 \sim r_0 + d\cos\Theta$ in phase and $r_0 \sim r_1 \sim r_2$ in amplitudes. It follows that:

$$\frac{\rho}{r_1} \sim \frac{\rho}{r_2} \sim \frac{\rho}{r_0} = \sin\Theta \tag{17}$$

$$\frac{z-d}{r_1} \sim \frac{z-d}{r_0} = \cos\Theta - \frac{d}{r_0} \tag{18}$$

$$\frac{z+d}{r_2} \sim \frac{z+d}{r_0} = \cos\Theta + \frac{d}{r_0} \tag{19}$$

The radiation field component in the spherical coordinate system can be obtained by the following formulas:

$$E_{0\Theta}^r(r_0,\Theta) = E_{0\rho}^r(r_0,\Theta)\cos\Theta - E_{0z}^r(r_0,\Theta)\sin\Theta \tag{20}$$

$$E_{0r}^r(r_0,\Theta) = E_{0\rho}^r(r_0,\Theta)\sin\Theta + E_{0z}^r(r_0,\Theta)\cos\Theta \tag{21}$$

The VED is the based element of an antenna. In practical applications, antennas are usually placed on the surface of the earth. In this case, $d/r_0 \sim 0, k_0 d \sim 0$, and the expressions of the three components are simplified as the following forms:

$$\begin{aligned} E_{0\Theta}^r(r_0,\Theta) = {} & -\frac{\omega\mu_0}{2\pi k_0}e^{ik_0r_0}\left\{-\frac{ik_0}{r_0\sin\Theta(\epsilon^*\sin\Theta+\cos\Theta)}\left[\left(2\cos\Theta+\sin\Theta\cos^2\Theta-\sin^3\Theta-1\right)\epsilon^*\sin^2\Theta\right.\right. \\ & \left.\left.+\cos\Theta\left(\sin^2\Theta\cos^2\Theta+\epsilon^*\cos\Theta-\sin^4\Theta\right)\right]+\frac{\epsilon^*\sin\Theta(\epsilon^*\cos\Theta-\sin\Theta)}{r_0^2(\epsilon^*\sin\Theta+\cos\Theta)^3}\right\} \\ & -\omega\mu_0\sqrt{\frac{2}{\pi r_0\sin\Theta}}e^{-i\frac{\pi}{4}}\sum_j\frac{A(\lambda_j)(\lambda_j^*)^{3/2}}{q'(\lambda_j^*)}\left[\cos\Theta-\frac{\lambda_j}{\gamma_0(\lambda_j)\sin\Theta}\right]e^{i\gamma_0(\lambda_j^*)r_0\cos\Theta+i\lambda_j^*r_0\sin\Theta} \end{aligned} \tag{22}$$

$$E_{0r}^{r}(r_0,\Theta) = -\frac{\omega\mu_0}{2\pi k_0}e^{ik_0r_0}\left[\frac{2ik_0\epsilon^*}{r_0(\epsilon^*\sin\Theta+\cos\Theta)}+\frac{\epsilon^*\sin\Theta(\epsilon^*\sin\Theta-\cos\Theta)}{r_0^2(\epsilon^*\sin\Theta+\cos\Theta)^3}\right]$$
$$-\omega\mu_0\sqrt{\frac{2}{\pi r_0\sin\Theta}}\,e^{-i\frac{\pi}{4}}\sum_j\frac{A(\lambda_j)(\lambda_j^*)^{3/2}}{q'(\lambda_j^*)}\left[\sin\Theta-\frac{\lambda_j}{\gamma_0(\lambda_j)\cos\Theta}\right]e^{i\gamma_0(\lambda_j^*)r_0\cos\Theta+i\lambda_j^*r_0\sin\Theta} \quad (23)$$

The radiation field on the surface is given by $\Theta = \pi/2$, $r_0 = \rho$.

$$E_{0\Theta}^{r}(\rho,\pi/2) = \frac{\omega\mu_0}{2\pi k_0}\,e^{ik_0\rho}\left(\frac{2ik_0}{\rho}+\frac{1}{\epsilon^{*2}\rho^2}\right)+\omega\mu_0\sqrt{\frac{1}{2\pi\rho}}\,e^{-i\frac{\pi}{4}}\sum_j\frac{A(\lambda_j)(\lambda_j^*)^{5/2}}{q'(\lambda_j^*)\gamma_0(\lambda_j^*)}\,e^{i\lambda_j^*\rho} \quad (24)$$

$$E_{0r}^{r}(\rho,\pi/2) = \frac{\omega\mu_0}{2\pi k_0}\,e^{ik_0\rho}\left(\frac{2ik_0}{\rho}+\frac{1}{\epsilon^{*2}\rho^2}\right)-\omega\mu_0\sqrt{\frac{1}{2\pi\rho}}\,e^{-i\frac{\pi}{4}}\sum_j\frac{A(\lambda_j)(\lambda_j^*)^{3/2}}{q'(\lambda_j^*)}\,e^{i\lambda_j^*\rho} \quad (25)$$

It is noted that these formulas consist of direct waves $(1/\rho)$, lateral waves $(1/\rho^2)$ and trapped-surface waves $(1/\rho^{-1/2})$, which is different from the three-layered case, in which the direct and ideal reflected (or image) fields vanish along the boundary. Following that, it is necessary to investigate the proportion of these waves.

3. NUMERICAL RESULTS

3.1. Piece-Wise Root-Finding Method

The approximate formulas are mentioned above. The roots of the pole equation (Eq. (26)) is shown in Fig. 2. We shift the contour around the branch lines at $\lambda = k_0$, $\lambda = k_1$, and $\lambda = k_2$. In this section, the main tasks are to determine the poles and present the numerical results of radiation field in a four-layered region.

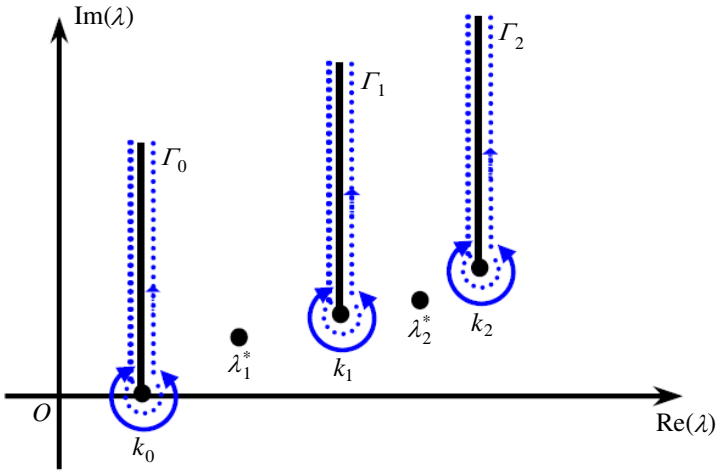

Figure 2. The roots of the pole equations.

The pole equation is in the following form.

$$q(\lambda) = k_1^2\gamma_0\left[\gamma_1k_2^2-\gamma_2k_1^2\tan(\gamma_1l_1)\tan(\gamma_2l_2)\right]-ik_0^2\gamma_1\left[\gamma_1k_2^2\tan(\gamma_1l_1)+\gamma_2k_1^2\tan(\gamma_2l_2)\right]=0 \quad (26)$$

The pole equation is more complex than the corresponding pole equation addressed in the three-layered case. It will be analyzed in the following four cases.

The first case is with $\lambda < k_0$, then γ_0, γ_1, and γ_2 are positive real numbers. Therefore, the pole equations are as follows.

$$\frac{\gamma_0}{k_0^2}\left[\frac{\gamma_1}{k_1^2}-\frac{\gamma_2}{k_2^2}\tan(\gamma_1l_1)\tan(\gamma_2l_2)\right]-i\frac{\gamma_1}{k_1^2}\left[\frac{\gamma_1}{k_1^2}\tan(\gamma_1l_1)+\frac{\gamma_2}{k_2^2}\tan(\gamma_2l_2)\right]=0 \quad (27)$$

Obviously, there is no pole in the interval $\lambda < k_0$.

In the second case with $k_0 < \lambda < k_1$, $\gamma_0 = i\sqrt{\lambda^2 - k_0^2} = i\gamma_0^{'}$, then $\gamma_0^{'}$, γ_1, and γ_2 are positive real numbers. Thus, the pole equation is obtained.

$$\frac{\gamma_0^{'}}{k_0^2}\left[\frac{\gamma_1}{k_1^2} - \frac{\gamma_2}{k_2^2}\tan(\gamma_1 l_1)\tan(\gamma_2 l_2)\right] - \frac{\gamma_1}{k_1^2}\left[\frac{\gamma_1}{k_1^2}\tan(\gamma_1 l_1) + \frac{\gamma_2}{k_2^2}\tan(\gamma_2 l_2)\right] = 0 \tag{28}$$

In the third case with $k_1 < \lambda < k_2$, $\gamma_i = i\sqrt{\lambda^2 - k_i^2} = i\gamma_i^{'}\,(i = 0, 1)$, then $\gamma_0^{'}$, $\gamma_1^{'}$, and γ_2 are positive real numbers.

$$-\frac{\gamma_0^{'}}{k_0^2}\left[\frac{\gamma_1^{'}}{k_1^2} - \frac{\gamma_2}{k_2^2}\tan(\gamma_1^{'} l_1)\tan(\gamma_2 l_2)\right] - \frac{\gamma_1^{'}}{k_1^2}\left[\frac{\gamma_1^{'}}{k_1^2}\tan(\gamma_1^{'} l_1) + \frac{\gamma_2}{k_2^2}\tan(\gamma_2 l_2)\right] = 0 \tag{29}$$

The poles can be determined by Eqs. (28) and (29).

In the forth case with $\lambda > k_2$, $\gamma_i = i\sqrt{\lambda^2 - k_i^2} = i\gamma_i^{'}(i = 0, 1, 2)$, then $\gamma_0^{'}$, $\gamma_1^{'}$, and $\gamma_2^{'}$ are positive real numbers.

$$-\frac{\gamma_0^{'}}{k_0^2}\left[\frac{\gamma_1^{'}}{k_1^2} + \frac{\gamma_2^{'}}{k_2^2}\tan(\gamma_1^{'} l_1)\tan(\gamma_2^{'} l_2)\right] - \frac{\gamma_1^{'}}{k_1^2}\left[\frac{\gamma_1^{'}}{k_1^2}\tan(\gamma_1^{'} l_1) + \frac{\gamma_2^{'}}{k_2^2}\tan(\gamma_2^{'} l_2)\right] = 0 \tag{30}$$

From Eq. (30), it is found that no pole exists in the interval $\lambda > k_2$.

3.2. Graphical Representations of $k_0 < k_1 < k_2 < k_3$

This section aims to present the numerical results in the case $k_0 < k_1 < k_2 < k_3$. In this paper, when the source and observation point are both near or on the boundary between the air and the dielectric layer, the propagation distance ρ is much larger than the height d and z so that conditions $d^2 \ll \rho^2$ and $z^2 \ll \rho^2$ are satisfied. Radiation field components $E_{0\Theta}(r_0, \Theta)$ varying with propagation distance are computed and shown in Fig. 3. The computation parameters are: $\epsilon_{1r} = 2.65$, $\epsilon_{2r} = 4$; $f = 100\,\text{MHz}$; and $d = z = 0\,\text{m}$. Meanwhile, changing the thickness of dielectric layers $l_1 = l_2 = 0.05\,\text{m}$; $l_1 = l_2 = 0.1\,\text{m}$; $l_1 = l_2 = 0.6\,\text{m}$; and $l_1 = 1.4\,\text{m}$, $l_2 = 0.8\,\text{m}$. Here, ϵ_{1r} and ϵ_{2r} are the relative permittivities of region 1 and region 2, respectively; f is the operating frequency; l_1 and l_2 are the corresponding thicknesses of dielectric layers. In Fig. 4, similar numerical results for the electric filed component $E_{0\Theta}^r$ varying with propagation distance are shown compared with different relative permittivities $\epsilon_{1r} = 2.65$, $\epsilon_{2r} = 4$; $\epsilon_{1r} = 3.15$, $\epsilon_{2r} = 4.5$; $\epsilon_{1r} = 4.35$, $\epsilon_{2r} = 5$; and $\epsilon_{1r} = 5.65$, $\epsilon_{2r} = 6$.

According to the results of Figs. 3 and 4, with the increase of propagation distance, the amplitude of the trapped surface wave decreases with $\rho^{-1/2}$ along the surface of dielectric layer. In addition, there are three sets of curves in which comparison is made between DRL wave (direct wave, ideal

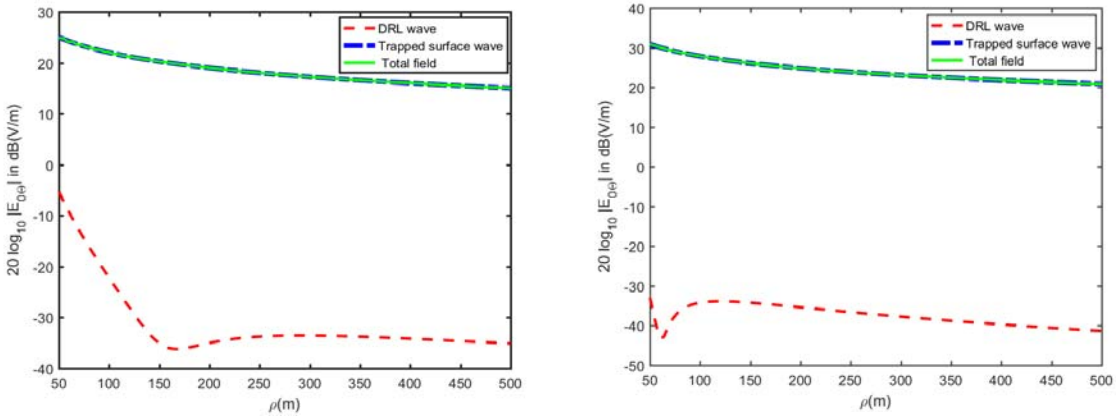

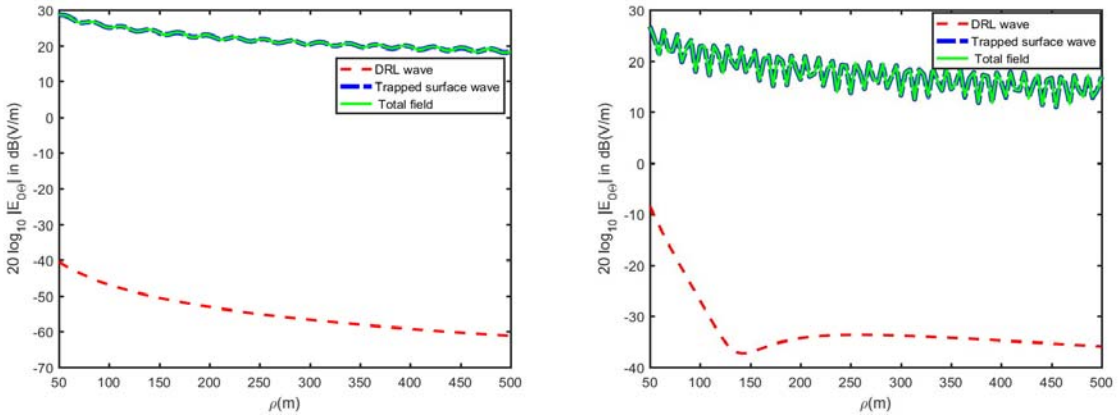

Figure 3. $E^r_{0\Theta}$ vs. propagation distance ρ with $f = 100\,\text{MHz}$, $\epsilon_{1r} = 2.65$, $\epsilon_{2r} = 4$, and $d = z = 0\,\text{m}$ under different dielectric layer thicknesses (a) $l_1 = l_2 = 0.05\,\text{m}$; (b) $l_1 = l_2 = 0.1\,\text{m}$; (c) $l_1 = l_2 = 0.6\,\text{m}$; (d) $l_1 = 1.4\,\text{m}$, $l_2 = 0.8\,\text{m}$.

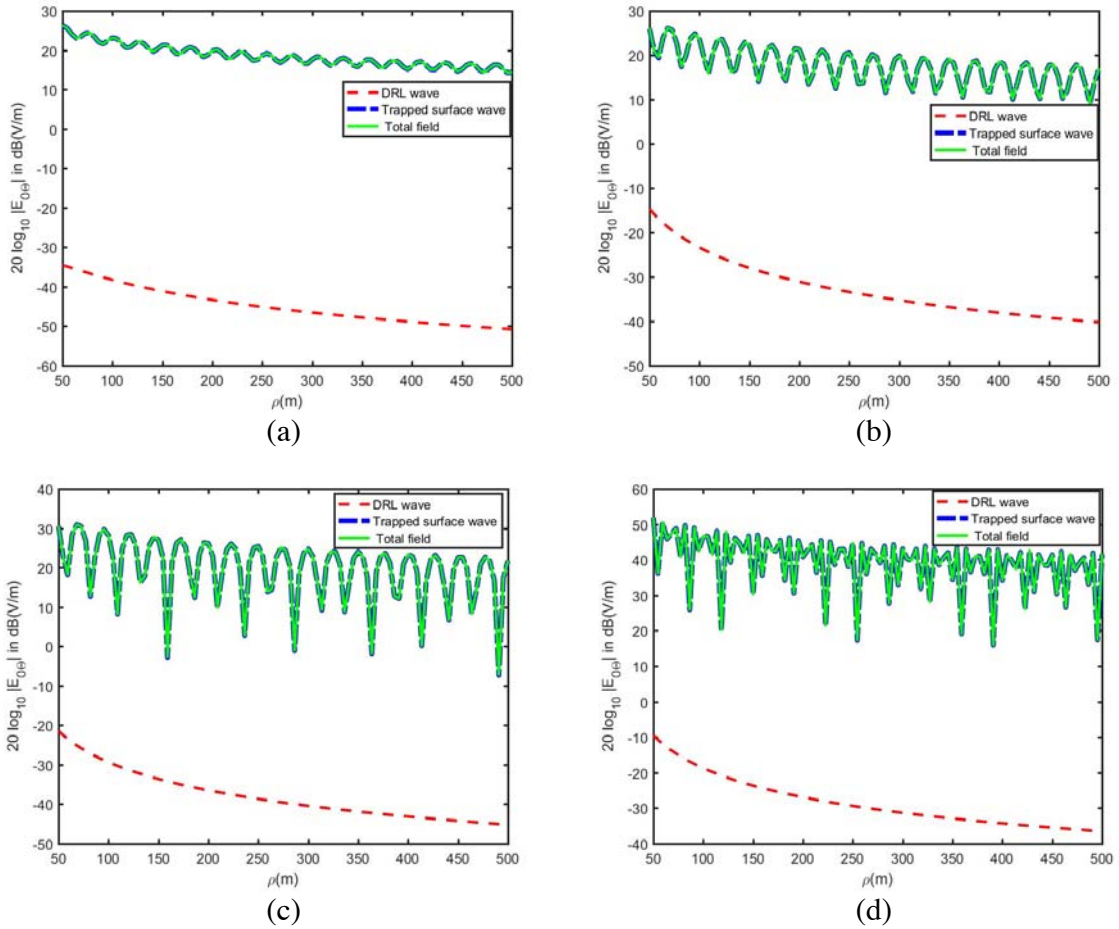

Figure 4. $E^r_{0\Theta}$ vs. ρ with $f = 100\,\text{MHz}$, $d = z = 0\,\text{m}$, and $l_1 = l_2 = 0.1\,\text{m}$ under different relative permittivities (a) $\epsilon_{1r} = 2.65$, $\epsilon_{2r} = 4$; (b) $\epsilon_{1r} = 3.15$, $\epsilon_{2r} = 4.5$; (c) $\epsilon_{1r} = 4.35$, $\epsilon_{2r} = 5$; (d) $\epsilon_{1r} = 5.5$, $\epsilon_{2r} = 6$.

reflect wave, and lateral wave), trapped surface wave, and total field wave, and the far field is mainly determined by trapped surface wave. Furthermore, under the dielectric layer's different thicknesses, there is a distinction between electric field components generated by VED in a four-layered region. The larger the thickness of dielectric layer is, the more obvious the interference phenomenon field component appears. It is noted that the electric field component $E^r_{0\Theta}$ has sharp interference with increasing relative permittivities.

The relationship between the field components and the angular degree (Θ) is studied. In Figs. 5 and 6, the numerical results for the electric field components $E^r_{0\Theta}(r_0, \Theta)$ and $E^r_0(r_0, \Theta)$ versus the angular degrees Θ are computed and shown, respectively. The computation parameters are: $f = 100\,\text{MHz}$, $\epsilon_{1r} = 2.65$, $\epsilon_{2r} = 4$, $l_1 = l_2 = 0.1\,\text{m}$, $r_0 = 20\,\text{m}$, and $d = z = 0\,\text{m}$. Considering the computation results, when $\Theta \leq 88°$, the dipole point or observation point has a certain distance between the boundary of the

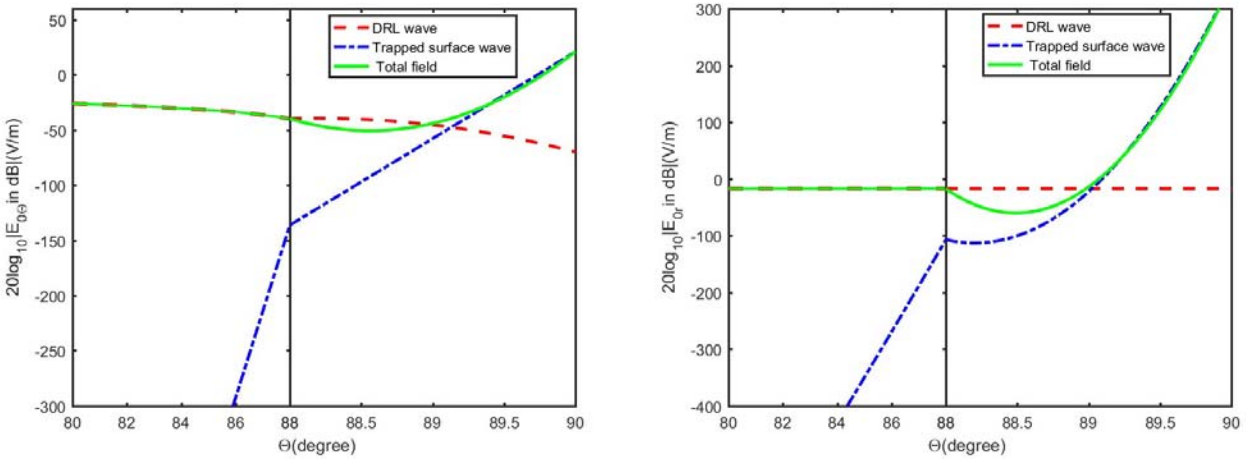

Figure 5. The electric components vs. the observation angle Θ with $f = 100\,\text{MHz}$, $\epsilon_{1r} = 2.65$, $\epsilon_{2r} = 4$, $d = z = 0\,\text{m}$, $r_0 = 20\,\text{m}$, and $l_1 = l_2 = 0.1\,\text{m}$ (a) $E^r_{0\Theta}$ vs. the observation angel Θ; (b) E^r_{0r} vs. the observation angle Θ.

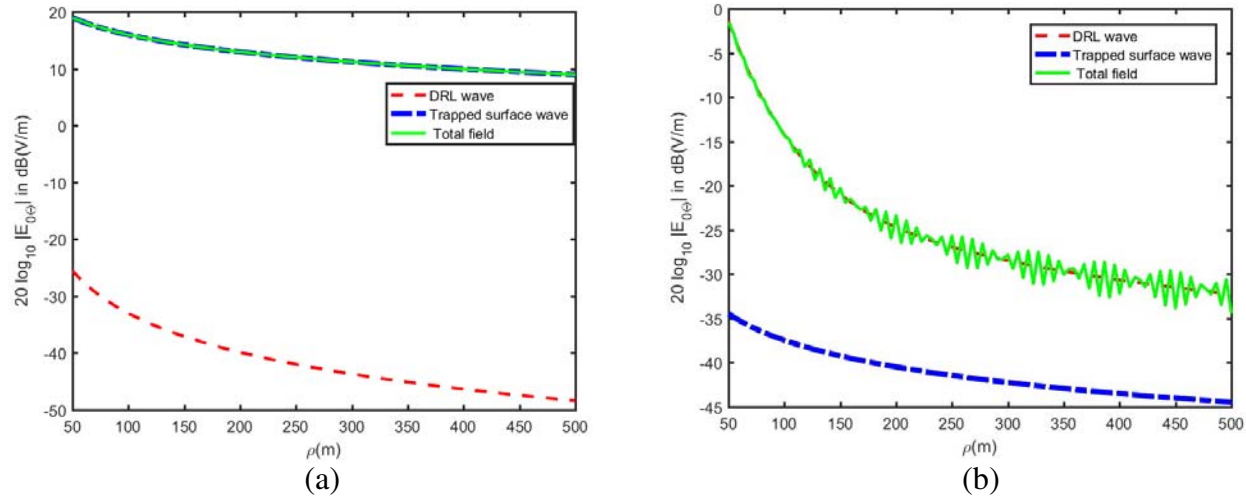

Figure 6. $E^r_{0\Theta}$ vs. propagation distance ρ with $f = 100\,\text{MHz}$, $l_1 = l_2 = 0.1\,\text{m}$, and $d = z = 0\,\text{m}$ under different conditions (a) $k_0 < k_1 < k_2 < k_3$; (b) $k_1 < k_0 < k_2 < k_3$.

air and the dielectric layer, and in this case, the trapped surface wave and DRL wave co-determine the total field. When $\Theta > 88°$, the dipole point and observation point are both close to or on air-dielectric boundary. In this condition, the trapped surface wave should be considered and is a major component of the total field.

3.3. Graphical Representations of $k_1 < k_0 < k_2 < k_3$

The electric filed $E^r_{0\Theta}$ as a function of the propagation distance is computed and shown under the condition $k_1 < k_0 < k_2 < k_3$ in Fig. 6. The parameters for computation are: $f = 100\,\text{MHz}$, $l_1 = l_2 = 0.1\,\text{m}$, and $d = z = 0\,\text{m}$. Based on the results, when the parameters of the dielectric layers do not satisfy the condition $k_0 < k_1 < k_2 < k_3$, the EM field does not effectively excite the trapped surface waves on the air-dielectric boundary. It is due to the changing of wave numbers that the pole equation has no solution, so that it degenerates into a two-layer situation. In a two-layered region, the total field is occupied by DRL, and the trapped surface wave vanishes along the boundary.

4. CONCLUSIONS

In this paper, approximate formulas have been obtained for the radiation field excited by a vertical electric dipole in the presence of a four-layered region. When the source and observation point are both near or on the air-electric boundary, the trapped surface wave attenuates with $\rho^{-1/2}$ along the boundary. Besides, the thicknesses of the dielectric layer and the relative permittivities have impact on the radiation field. Furthermore, the cutoff point of angular degrees is $\Theta = 88°$. When $\Theta \leq 88°$, the total field is determined by DRL wave and trapped surface wave. Otherwise, the trapped surface wave is the major component of total field. Moreover, different cases are examined to evaluate the proportion of the trapped surface wave and DRL wave. When the wave numbers do not meet the condition $k_0 < k_1 < k_2 < k_3$, the radiation field is occupied by DRL wave.

ACKNOWLEDGMENT

This work is supported by the open project of Zhejiang Provincial Key Laboratory of Advanced Microelectronic Intelligent Systems and Applications (ZJUAMIS2001). The authors are grateful to all referees for their constructive comments and suggestions in improving the quality of this paper.

REFERENCES

1. Sommerfeld, A. N., "Propagation of waves in wireless telegraphy," *Ann. Phys. (Leipzig)*, Vol. 28, 665–737, 1909.
2. Wait, J. R., *Electromagnetic Waves in Stratified Media: Revised Edition Including Supplemented Material*, Elsevier, Amsterdam, 2013.
3. King, R. W. P., M. Owens, and T. T. Wu, *Lateral Electromagnetic Waves: Theory and Applications to Communications, Geophysical Exploration, and Remote Sensing*, Springer Science and Business Media, Berlin, 2012.
4. Wait, J. R., "Comment on "The electromagnetic field of a vertical electric dipole in the presence of a three-layered region" by R. W. P. King and S. S. Sandler," *Radio Science*, Vol. 33, 251–253, 1998.
5. Mahmoud, S. F., R. W. P. King, and S. S. Sandler, "Remarks on "The electromagnetic field of a vertical electric dipole over the Earth or sea" [and reply]," *IEEE Transactions on Antennas and Propagation*, Vol. 47, 1745–1747, 1999.
6. King, R. W. P., "The electromagnetic field of a horizontal electric dipole in the presence of a three-layered region," *Journal of Applied Physics*, Vol. 69, 7987–7995, 1991.
7. King, R. W. P., "The electromagnetic field of a horizontal electric dipole in the presence of a three-layered region: Supplement," *Radio Science*, Vol. 74, 4845–4848, 1993.

8. King, R. W. P. and S. S. Sandler, "The electromagnetic field of a vertical electric dipole in the presence of a three-layered region," *Radio Science*, Vol. 29, 97–113, 1994.
9. Zhang, H. Q. and W. Y. Pan, "Electromagnetic field of a vertical dipole on a perfect conductor coated with a dielectric layer," *Radio Science*, Vol. 37, 1–7, 2002.
10. Zhang, H. Q., K. Li, and W. Y. Pan, "The electromagnetic field of a vertical dipole on the dielectric-coated imperfect conductor," *Journal of Electromagnetic Waves and Applications*, Vol. 18, 1305–1320, 2004.
11. Zhang, H.-Q., W.-Y. Pan, K. Li, and K.-X. Shen, "Electromagnetic field for a horizontal electric dipole buried inside a dielectric layer coated high lossy half space," *Progress In Electromagnetics Research*, Vol. 50, 163–186, 2005.
12. Liu, L., K. Li, and W.-Y. Pan, "Electromagnetic field from a vertical electric dipole in a four-layered region," *Progress In Electromagnetics Research B*, Vol. 8, 213–241, 2008.
13. Xu, Y. H., K. Li, and L. Liu, "Electromagnetic field of a horizontal electric dipole in the presence of a four-layered region," *Progress In Electromagnetics Research*, Vol. 81, 371–391, 2008.
14. Li, K., *Electromagnetic Fields in Stratified Media*, Springer Science & Business Media, Hangzhou, 2009.
15. Li, L. W., T. S. Yeo, P. S. Kooi, and M. S. Leong, "Radio wave propagation along mixed paths through a four-layered model of rain forest: An analytic approach," *IEEE Transactions on Antennas and Propagation*, Vol. 46, 1098–111, 1998.
16. Li, L. W., C. K. Lee, T. S. Yeo, and M. S. Leong, "Wave mode and path characteristics in a four-layered anisotropic forest environment," *IEEE Transactions on Antennas and Propagation*, Vol. 52, 2445–2455, 2004.
17. Lu, Y. L., Y.-L. Wang, Y. H. Xu, and K. Li, "Electromagnetic field of a horizontal electric dipole buried in a four-layered region," *Progress In Electromagnetics Research B*, Vol. 16, 247–275, 2009.
18. Zou, L. L., "On the use of lateral wave for the interlayer debonding detecting in an asphalt airport pavement using a multistatic GPR system," *IEEE Transactions on Geoscience and Remote Sensing*, 1–10, 2020.
19. Lin, Z. H., Z. T. Chen, and K. Li, "Radiation patterns of a horizontal electric dipole in a four-layered region and applications for microstrip antennas," *Journal of Electromagnetic Waves and Applications*, 1–18, 2020.